

# Studies toward the structural optimization of new brazilzone-related trypanocidal 1,3,4-thiadiazole-2-arylhydrazone derivatives

Samir A. Carvalho,<sup>a</sup> Francisco A. S. Lopes,<sup>b</sup> Kelly Salomão,<sup>b</sup> Nelilma C. Romeiro,<sup>c</sup> Solange M. S. V. Wardell,<sup>a</sup> Solange L. de Castro,<sup>b</sup> Edson F. da Silva<sup>a</sup> and Carlos A. M. Fraga<sup>c,\*</sup>

<sup>a</sup>Fundação Oswaldo Cruz, Instituto de Tecnologia em Fármacos - Far-Manguinhos, Laboratório de Síntese IV, 21041-250 Rio de Janeiro, RJ, Brazil

<sup>b</sup>Laboratório de Biologia Celular, Instituto Oswaldo Cruz, FIOCRUZ, Rio de Janeiro, RJ, Brazil

<sup>c</sup>LASSBio – Laboratório de Avaliação e Síntese de Substâncias Bioativas, Faculdade de Farmácia, Universidade Federal do Rio de Janeiro, PO Box 68023, 21941-902 Rio de Janeiro, RJ, Brazil

Received 30 June 2007; revised 11 September 2007; accepted 13 September 2007  
Available online 18 September 2007

**Abstract**—Megazol is a highly active compound against *Trypanosoma cruzi*, and has become a core structure for the design of new trypanocidal agents. Recently, we have identified the new potent trypanocide agent Brazilzone A, which presents an IC<sub>50</sub> twofold more potent than the prototype megazol. This result has encouraged us to further explore structurally-related 1,3,4-thiadiazole-2-arylhydrazone derivatives, in order to get a better understanding of their structural and antiprotozoal activity relationships. Herein we report the synthesis and trypanocidal profile of thirteen new Brazilzone A analogues, which supported the construction of 3D-QSAR models used for its structural optimization.

© 2007 Elsevier Ltd. All rights reserved.

## 1. Introduction

Chagas' disease represents one of the most important parasitic infections in Latin America, affecting 16–18 million people currently infected by the hemoflagellate protozoan *Trypanosoma cruzi*.<sup>1</sup> Currently available drugs have limited efficacy in the prevalent chronic stage of the disease and frequent toxic side effects.<sup>2</sup> Few compounds have the high efficiency of megazol (**1**, Fig. 1), a 5-nitroimidazole derivative synthesized in 1968 by Berkelhammer and Asato<sup>3</sup> as an antimicrobial agent. Megazol (**1**) was later characterized by Brener's group<sup>4</sup> as a powerful trypanocide agent. It is worth mentioning that it is active against different strains of the parasite and has great effectiveness in monkeys even in the chronic stage.<sup>5</sup>

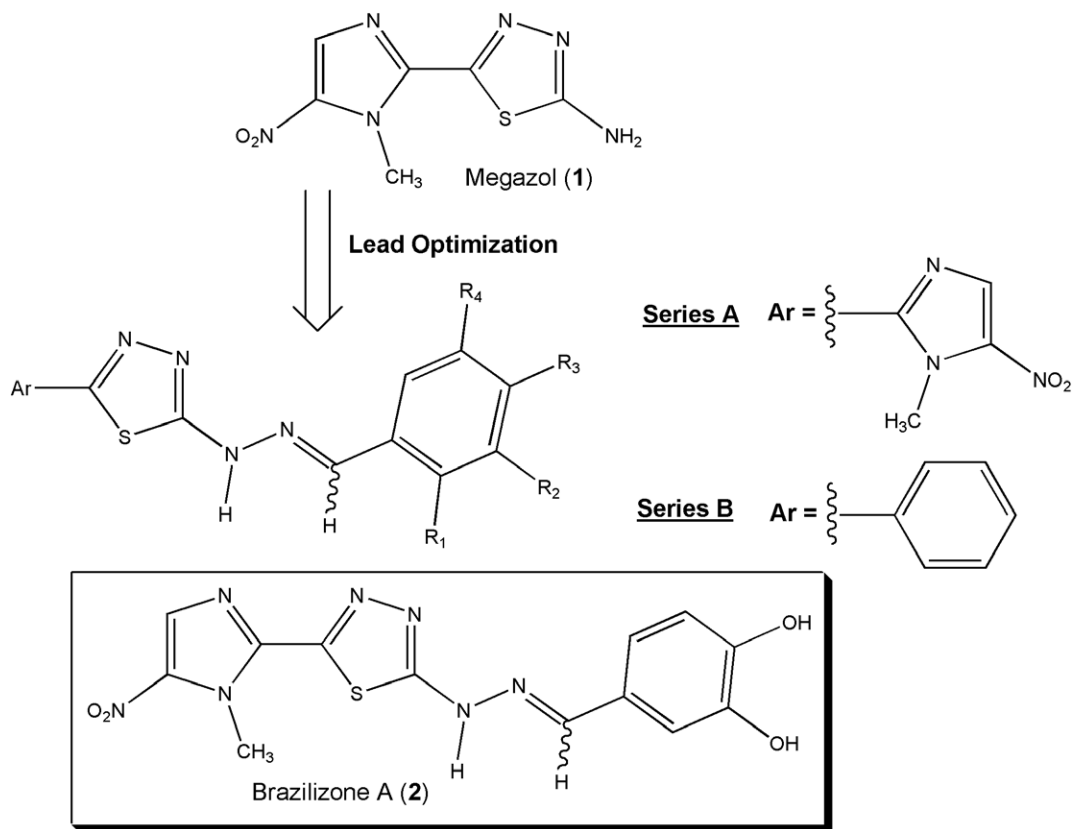
For this reason, megazol (**1**) was considered as an alternative lead-compound for the treatment of the Chagas'

Disease, whose expressive antiprotozoal profile was associated with the interference with parasite oxygen metabolism, as well as its role as trypanothione scavenger.<sup>6–8</sup> However, the mechanism involved in the trypanocide activity of **1** is narrowly dependent of the bioformation of reactive intermediate species,<sup>9,10</sup> produced by the nitro group reduction, which interacts with DNA producing mutagenicity.<sup>11,12</sup> In spite of this limitation for the therapeutical use of **1**, it has been exploited as template for the design of new safer antichagasic prototypes.<sup>13–16</sup>

Considering this panorama and trying to circumvent this undesirable profile, several megazol analogues belonging to a new class of 1,3,4-thiadiazole-2-arylhydrazone derivatives of series *A* and *B* (Fig. 1) have been designed and synthesized as attractive antichagasic drug candidates. Due to the hypothesis that the introduction of a radical scavenger subunit linked to the heterocyclic scaffold of (**1**) could modulate the production of toxic nitro anion radical species, they could potentially avoid mutagenic properties. The arylhydrazone derivative named brazilzone A (**2**, Fig. 1, IC<sub>50</sub> = 5.3 μM) was the most active compound against trypomastigote forms of *T. cruzi*, being twofold more potent than the proto-

**Keywords:** Megazol; 1,3,4-Thiadiazole-2-arylhydrazone; *Trypanosoma cruzi*; Chagas' disease; Chemotherapy; CoMFA model.

\* Corresponding author. Tel.: +55 21 22609192; fax: +55 21 25626478; e-mail: cmfraga@pharma.ufrj.br



**Figure 1.** Brazilizone A (2) and other 1,3,4-thiadiazole-2-aryllhydrazone derivatives of series A and B.

type megazol (1,  $IC_{50} = 9.9 \mu\text{M}$ ) in the same experimental protocol.<sup>17</sup>

These initial results encouraged us to give continuity to this approach, and herein we report the synthesis and trypanocidal profile of thirteen new brazilizone A analogues, in order to compose the congeneric series of 1,3,4-thiadiazole-2-aryllhydrazone derivatives and support the construction of 3D-QSAR models able to guide the structural design of new optimized trypanocidal agents. In addition, theoretical pharmacokinetic calculations (Lipinski's rule of five) have been made in order to support further in vivo studies.

## 2. Results and discussion

### 2.1. Chemistry

The new 1,3,4-thiadiazole-2-aryllhydrazone derivatives (3–15) have been obtained by the method described previously,<sup>17</sup> exploiting megazol (2) as starting material and the heteroaryl hydrazine (16, Table 1) as key intermediate. The target hydrazone derivatives (3–15) were obtained, in good yields, by acid catalyzed condensation of the hydrazine (16) with the corresponding aromatic aldehydes (ArCHO) in ethanol, as described in Table 1.

The analysis of the <sup>1</sup>H NMR spectra and HPLC chromatograms of the synthesized compounds (3–15) was consistent with the major or exclusive presence of one

geometric isomer at C=N bond level, which displayed the imine hydrogen signal ranging from 8.22 to 8.28 ppm.

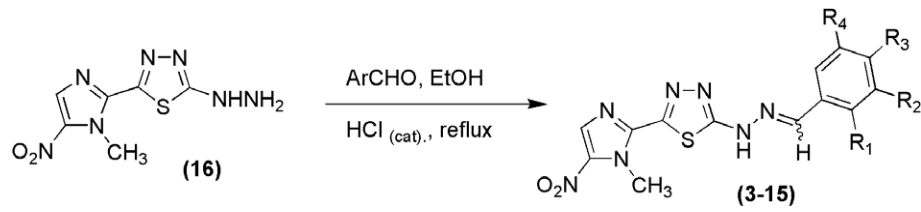
In order to assure unambiguously the relative configuration of the major diastereomer obtained during the synthesis of brazilizone derivatives, essential to the understanding of the biological results and perform adequately the proposed 3D-QSAR studies, we have selected the unsubstituted compound of series B, that is, (17, Fig. 2),<sup>17</sup> as a model to investigate the geometric isometry of both series by X-ray diffraction.

The atom arrangements with selected geometric parameters are shown in Figure 3. The overall molecule is nearly planar with the angles between the best planes of the 1,3,4-thiadiazole ring, phenyl rings, and link chain ranging from 0.95 (0.42) to 9.99 (0.39)°.

Hydrogen bonds involving N2 and N3 lead to the formation of symmetrical dimers. In addition to these strong H-bonds, weaker intramolecular C–H–S interactions cement the conformation as shown in Figure 3. Furthermore, Platon analysis<sup>18</sup> reveals a number of  $\pi$ - $\pi$  type intermolecular interactions, including  $\pi$ - $\pi$ , and C–H- $\pi$  (Fig. 3).

### 2.2. Trypanocidal activity

The antitrypanosomal profile of the new 1,3,4-thiadiazole-2-aryllhydrazones of nitro-imidazole series A (3–15)

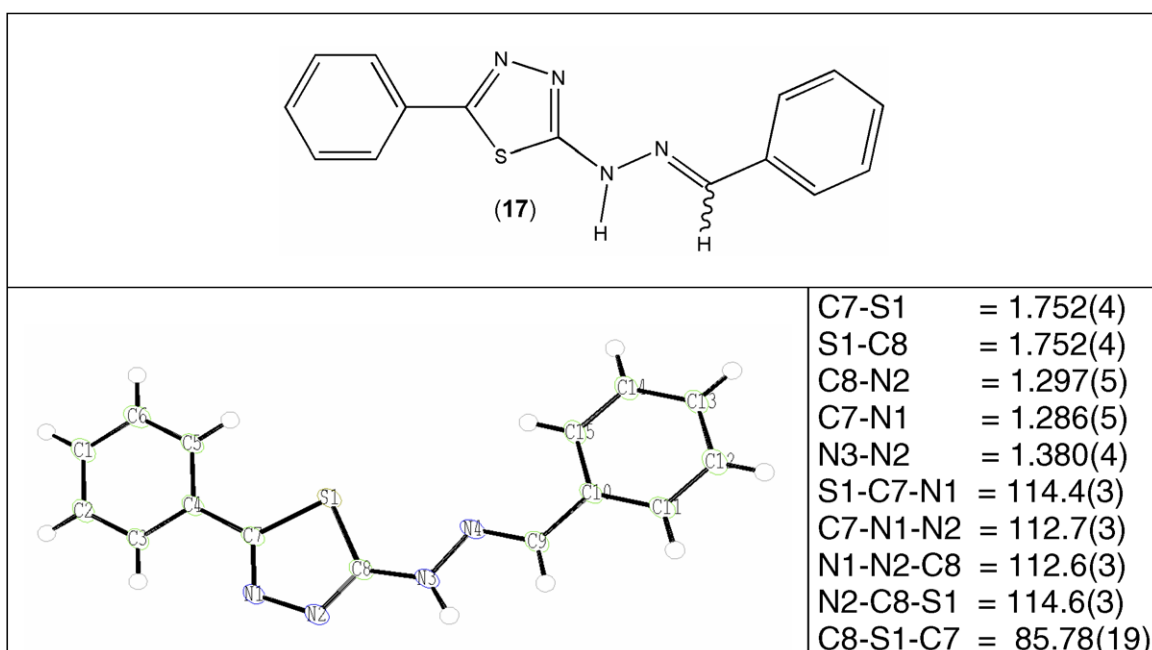
**Table 1.** Physical, structural, and biological properties of the 1,3,4-thiadiazole-2-arylhydrazone derivatives (3–15)


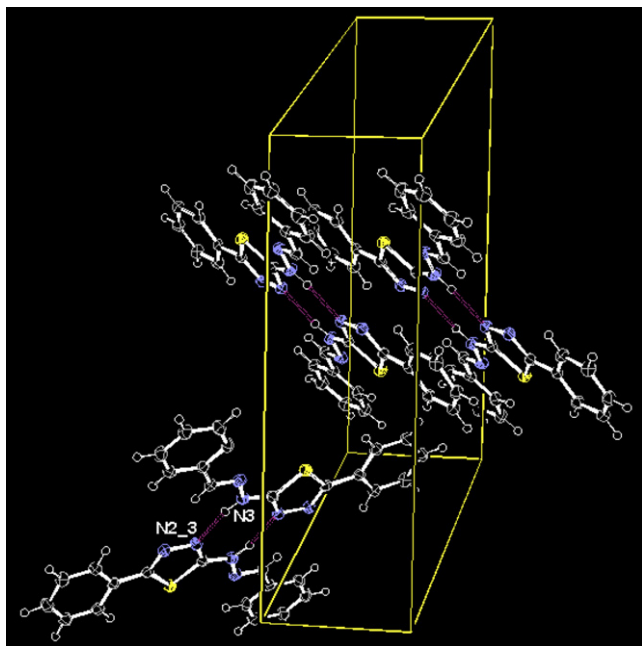
Compound	R <sub>1</sub>	R <sub>2</sub>	R <sub>3</sub>	R <sub>4</sub>	Molecular formula <sup>b</sup>	MW	Yield (%)	Mp (°C)	Diastereoselection <sup>c</sup> (ratio)	IC <sub>50</sub> (μM) <sup>d</sup>
Megazol (1) <sup>a</sup>	—	—	—	—	—	—	—	—	—	9.9 ± 0.8
Brazilizone A (2) <sup>a</sup>	H	OH	OH	H	C <sub>13</sub> H <sub>11</sub> N <sub>7</sub> O <sub>4</sub> S	316.0	66	299–300	E	5.3 ± 0.6
3	H	NO <sub>2</sub>	H	H	C <sub>13</sub> H <sub>11</sub> ClN <sub>8</sub> O <sub>4</sub> S	410.8	77	295–296	E	48.2 ± 3.2
4	H	OH	H	H	C <sub>13</sub> H <sub>12</sub> ClN <sub>7</sub> O <sub>3</sub> S	381.8	83	299–300	E	73.9 ± 5.2
5	OH	H	H	OH	C <sub>13</sub> H <sub>12</sub> ClN <sub>7</sub> O <sub>4</sub> S	397.8	89	302	E	140.0 ± 8.9
6	Cl	H	H	H	C <sub>13</sub> H <sub>11</sub> Cl <sub>2</sub> N <sub>7</sub> O <sub>3</sub> S	400.2	71	331–332	E	140.3 ± 18.7
7	H	Cl	H	H	C <sub>13</sub> H <sub>11</sub> Cl <sub>2</sub> N <sub>7</sub> O <sub>3</sub> S	400.2	82	286–287	E	186.9 ± 15.1
8	OH	OH	H	H	C <sub>13</sub> H <sub>12</sub> ClN <sub>7</sub> O <sub>4</sub> S	397.8	71	317	E	309.3 ± 23.6
9	NO <sub>2</sub>	H	NO <sub>2</sub>	H	C <sub>13</sub> H <sub>10</sub> ClN <sub>8</sub> O <sub>6</sub> S	455.8	90	311	E	330.2 ± 6.8
10	H	Br	H	H	C <sub>13</sub> H <sub>11</sub> BrClN <sub>7</sub> O <sub>2</sub> S	444.7	83	306–307	E	727.6 ± 22.4
11	NO <sub>2</sub>	H	H	H	C <sub>13</sub> H <sub>11</sub> ClN <sub>8</sub> O <sub>4</sub> S	410.8	80	327–328	E	726.2 ± 38.2
12	Cl	H	Cl	H	C <sub>13</sub> H <sub>10</sub> Cl <sub>3</sub> N <sub>7</sub> O <sub>3</sub> S	434.7	84	314	E/Z (7/3)	793.5 ± 65.0
13	Br	H	H	H	C <sub>13</sub> H <sub>11</sub> BrClN <sub>7</sub> O <sub>2</sub> S	444.7	80	311–312	E/Z (7/3)	900.0 ± 11.5
14	Cl	Cl	H	H	C <sub>13</sub> H <sub>10</sub> Cl <sub>3</sub> N <sub>7</sub> O <sub>3</sub> S	434.7	87	328–329	E	1208.8 ± 180.3
15	H	NO <sub>2</sub>	OH	OCH <sub>3</sub>	C <sub>14</sub> H <sub>12</sub> N <sub>8</sub> O <sub>6</sub> S	420.4	93	275–276	E	19.0 ± 3.3

<sup>a</sup> Data obtained from Ref. 17.<sup>b</sup> The analytical results for C, H, N, S were within ± 0.4% of calculated values.<sup>c</sup> Data obtained at 500 MHz, using DMSO-*d*<sub>6</sub> as solvent and confirmed by HPLC using a Rexchrom 5 μm RP-18 column (125 × 4.6 mm) and a mixture of methanol–water (7:3 v/v) as eluent at a flow rate of 1 mL/min.<sup>d</sup> Means ± standard deviation of at least four separated experiments performed with trypomastigote forms of *T. cruzi*.

was carried out using the trypomastigote form of *T. cruzi* obtained from mice intraperitoneally inoculated with 10<sup>5</sup> parasites of the Y strain.<sup>17,19</sup> The results were analyzed by plotting % lysis of *T. cruzi* against the concentration of the test-compound. The values of IC<sub>50</sub>

corresponded to the concentration that led to 50% lysis of the parasite and are summarized in Table 1. The most active hydrazone compounds of this new series were 5-nitrovanillyl (15) and 3-nitrophenyl (3) derivatives. They exhibit IC<sub>50</sub> = 19.0 and 48.2 μM, respectively, both

**Figure 2.** Molecular structure and selected geometric parameters, (Å, °), for the arylhydrazone derivative (17). Ellipsoids, for non-hydrogen atoms, are drawn at the 50% probability level; H atoms are drawn as arbitrary spheres.



**Figure 3.** Hydrogen bonding and packing arrangements of the 1,3,4-thiadiazole-2-arylhydrazone derivative (**17**).

being less potent than the prototype Brazilizone A ( $IC_{50} = 5.3 \mu M$ ). These results coupled with the investigation of the bioprofile of other heteroarylhydrazone compounds (**4–14**), containing substituents with different stereo electronic contributions in  $R_1$ ,  $R_2$ ,  $R_3$ , and  $R_4$  of the phenyl ring attached to the imine double bond, confirmed the pharmacophoric character of the catechol or equivalent subunits adequately placed in compound (**2**) and in the parent analogue (**15**). In spite of the reduced antitrypanosomal activity, results obtained on some newly synthesized compounds (**3–14**), when used together with results from 1,3,4-thiadiazolyhydrazones previously reported,<sup>17</sup> were essential in order to construct a CoMFA model able to explain the stereoelectronic features required by the target bioreceptor in *T. cruzi*.

### 2.3. 3D-QSAR studies: CoMFA

3D-QSAR analysis was performed using the CoMFA module implemented in SYBYL 7.3 package.<sup>20,21</sup> The heteroarylhydrazone derivatives (**2–15**) (Table 1) were used in the 3D-QSAR studies while 10 additional analogues were retrieved from a previous report,<sup>17</sup> summing up 20 compounds of the training set and 3 compounds of the test set, which have been left out of model construction for external validation. CoMFA steric and electrostatic fields were the independent variables and  $pIC_{50}$  values ( $-\log IC_{50}$ ), described in Table 1 and in the published work,<sup>17</sup> were the dependent variables in the linearization process.

In the alignment step, manual atom fitting to the most active derivative (**2**), used as template, was performed as indicated in Figure 4.

Only models having a value of cross-validated  $r^2$  ( $q^2$ ) above 0.5 were considered (Table 2), in agreement with

reports in the literature that show that models with  $q^2$  values greater than 0.5–0.6 are useful for the prediction of new biologically active molecules.<sup>22</sup>

The best CoMFA models (I–III) showed good statistical parameters (Table 2). However, model III, with  $q^2 = 0.723$ , SEP = 0.386,  $r^2 = 0.895$ , SEE = 0.238, and  $F = 45.264$ , has been selected as the most representative of the SAR of the set of studied analogues (Table 2).

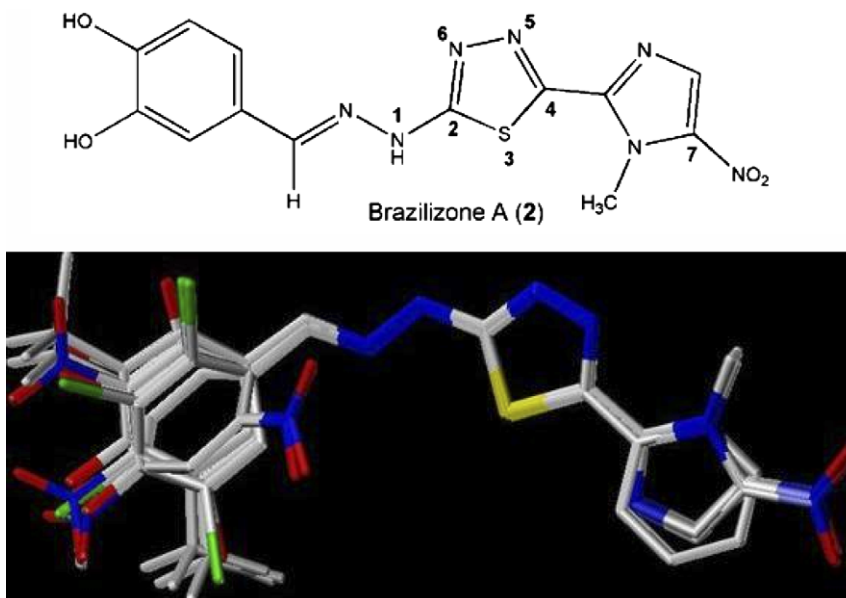
CoMFA steric and electrostatic contour maps of Model III and the two most active arylhydrazone derivatives reported in this work, that is, Brazilizone A (**2**) and its nitrovanillyl analogue (**15**), named Brazilizone N, are depicted in Figure 5.

The steric contour maps are shown as green and yellow polyhedra in Figure 5a. The green contours indicate molecular regions where steric bulk will increase biological activity, while the yellow contours indicate molecular regions where steric bulk will decrease activity. The electrostatic contour maps (Fig. 5b) show red polyhedra in molecular regions where electron-rich groups lead to increase in biological activities. On the other hand, blue polyhedral are indicative of areas where electron-poor groups increase activity.

From the 3D-QSAR studies, it is clear that the phenyl ring attached to the aryl-hydrazone moiety can bear bulky groups without jeopardizing biological activity, as had already been seen in our previous work.<sup>17</sup> However, *ortho* effects in general seem to have a deleterious effect on the biological activity, as exemplified by compounds **11–14** that would possibly occupy the sterically forbidden region represented by the yellow contour close to position 2 ( $R_1$ ) of brazilizone A (Fig. 5a, Table 1). This hypothesis is illustrated in Figure 5c, where compound **14** is superimposed in the CoMFA steric contour map, with the *ortho*-chlorine atom occupying a sterically forbidden region (yellow). Altogether, these results suggest that conformational restriction of the phenyl ring generated by bulky substituents in positions 3 ( $R_2$ ) and 5 ( $R_4$ ) is activity-enhancing.

The inspection of brazilizone A (**2**) superimposed to the steric contour map indicates that bulky substituents at position 4 ( $R_3$ ) of the phenyl ring are supported (Fig. 5a), as exemplified by compound **15** (Table 1).

The inspection of the electrostatic contour map sheds light on the molecular basis of the activity of the present series of brazilizone A analogues, since the hydroxyl group in position 4 ( $R_3$ ) of the phenyl ring occupies a region that requires electron-rich groups, that is, the oxygen atom present in the hydroxyl moiety (Fig. 5b). The blue contour map around positions 3 ( $R_2$ ) and 4 ( $R_3$ ) of the phenyl ring is close to the electron-poor hydrogen atom attached to the hydroxyl groups located in these positions. In some molecules, that is, compound **8**, the contribution of this map to biological activity may be more important due to intramolecular hydrogen bonding between the vicinal hydroxyl groups, increasing the net positive charge in one of the hydrogen atoms. This



**Figure 4.** Atoms used to align 1,3,4-thiadiazole-2-arylhydrazone derivatives using brazilizone A (**2**) as template and the stereo view of the aligned molecules used in the CoMFA study.

**Table 2.** PLS results for the best CoMFA models obtained for trypanocidal 1,3,4-thiadiazole-2-arylhydrazone derivatives

CoMFA model	PLS analysis					
	$q^2$	$n$	SEP	$r^2$	SEE	$F$ value
I	0.681 <sup>a</sup>	3	0.414	0.871	0.264	35.876
II	0.696 <sup>a</sup>	3	0.404	0.888	0.246	42.077
III	0.723 <sup>a</sup>	3	0.386	0.895	0.238	45.264

$q^2$  Leave-one-out (LOO) cross-validated correlation coefficient.

$n$  Optimum number of components.

SEP Standard error of prediction.

$r^2$  Non cross-validated correlation coefficient.

SEE Standard error of estimate.

$F$  Fischer's test value.

<sup>a</sup> Cutoff contributions have been truncated to:  $\pm 30$  (steric) and  $\pm 45$  (electrostatic) kcal/mol<sup>-1</sup>.

blue region may also be occupied by the electron-poor nitrogen atom pertaining to the nitro group of brazilizone N (**15**) and compound **3**, both in position 3 (**R**<sub>2</sub>) (Table 1).

Another interesting observation is that the best model (Model III, Table 2) is able to differentiate compounds that bear a nitro imidazole group from the ones that have a phenyl ring (from our previous work)<sup>17</sup> as can be seen from the red contours around the oxygen atoms pertaining to the nitro group of brazilizone A (Fig. 5b). This data reinforces the importance of the nitro group for the antitrypanosomal profile of this series of compounds. Furthermore, our CoMFA studies have shown that the steric and electrostatic requirements of their bioreceptor are clearly dependent on the phenyl ring orientation and on the steric and electronic characteristics of the substituents.

#### 2.4. Prediction of in vivo absorption: Lipinski's rule of five

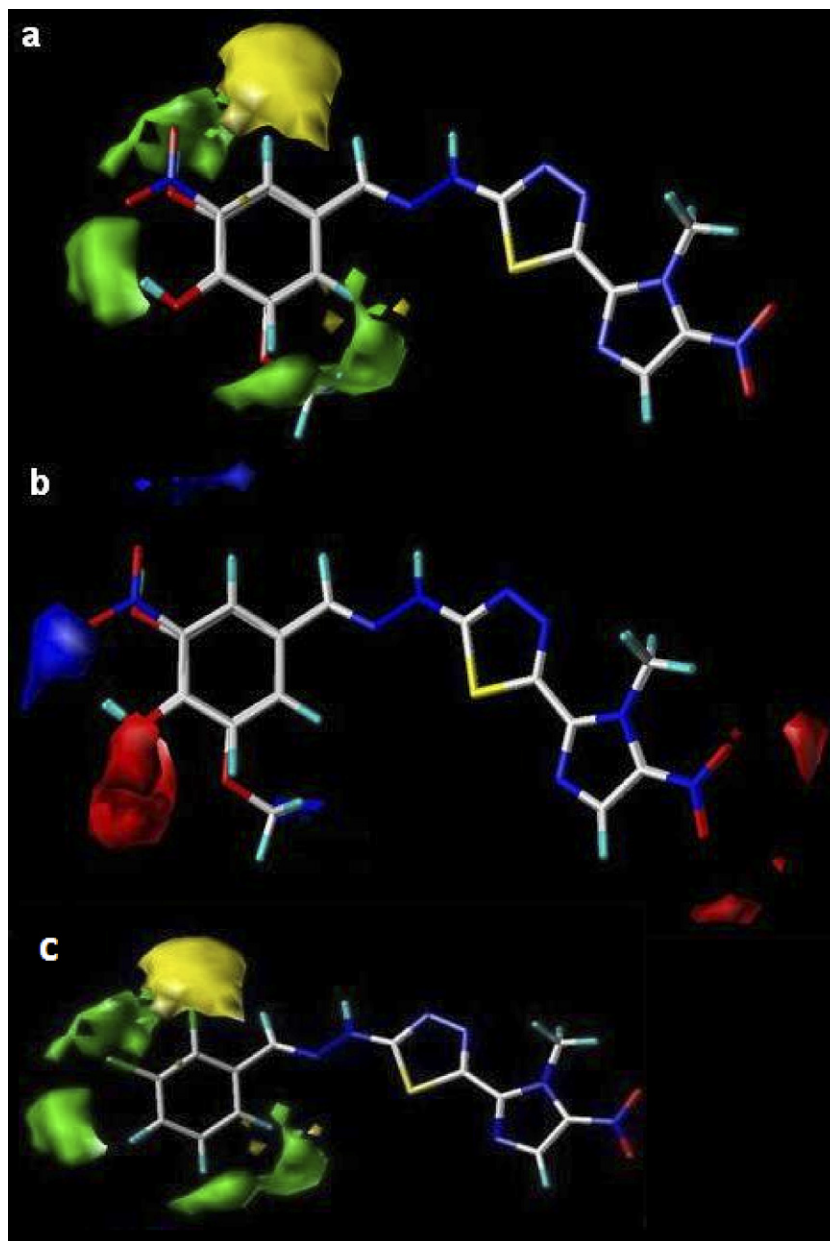
In addition to 3D-QSAR, in vivo absorption capabilities of two promising heteroarylhydrazone derivatives from

this series were tentatively assessed by means of theoretical calculations following Lipinski's rule of five,<sup>23,24</sup> that establishes that a compound administered orally will more likely have good absorption or permeation if it satisfies the following criteria: (a) hydrogen bond donors  $\leq 5$  (OH and NH groups); (b) hydrogen bond acceptors  $\leq 10$  (N and O atoms); (c) molecular weight  $< 500$ ; (d) calculated  $\log P$  (Clog  $P$ )  $< 5$ . This approach has been widely used as a filter for substances that would likely be further developed in drug design programs. The results of the calculations for brazilizone A (**2**) and brazilizone N (**15**) showed that both compounds have a potential for good in vivo absorption, since then satisfied Lipinski's rule of five without violations (Table 3).

### 3. Conclusions

Among the new heteroarylhydrazone derivatives (**3–15**), designed by stereo electronic modifications of substituents attached to the phenyl ring of the prototype brazilizone A (**2**), was discovered 4-hydroxy-3-methoxy-5-nitrobenzaldehyde [5-(1-methyl-5-nitro-1H-imidazol-2-yl)-





**Figure 5.** View of the CoMFA steric (a) and electrostatic (b) field contour maps for model III superimposed with brazilizone A (**2**) and brazilizone N (**15**). (c) View of less active compound (**14**) inside the CoMFA steric map.

1,3,4-thiadiazol-2-yl]hydrazine (**15**), named brazilizone N, which showed to present good in vitro trypanocidal profile. Additionally, the 3D-QSAR CoMFA model developed for this series of trypanocidal brazilizone analogues gave insight into the influence of various structural features for the biological activity. Finally, since our 3D-QSAR analyses showed that predicted activities correlate well with experimental  $IC_{50}$  values, suggesting that the 3D-QSAR models are reliable, this study may be considered as a powerful tool in design-

ing and forecasting more efficacious anti-chagasic lead-candidates.

## 4. Experimental

### 4.1. General procedures

Melting points were determined on a Buchi apparatus and are uncorrected. Infrared spectra were recorded

**Table 3.** Molecular descriptors for Lipinski's rule of some 1,3,4-thiadiazole-2-arylhydrazone derivatives

Compound	MW	CLOGP	Hydrogen bond donors	Hydrogen bond acceptors	Satisfies the rule of five?
Brazilizone A ( <b>2</b> )	316.0	1.92	3	8	Yes
Brazilizone N ( <b>15</b> )	420.4	2.08	2	10	Yes

on a Thermo Nicolet Nexus 670 spectrometer in potassium bromide pellets and frequencies are expressed in  $\text{cm}^{-1}$ .  $^1\text{H}$  NMR spectra were recorded, at room temperature, on a Bruker Avance 500 spectrometer operating at 500 MHz ( $^1\text{H}$ ). Chemical shifts are reported in ppm ( $\delta$ ) downfield from tetramethylsilane used as internal standard.

The progress of all reactions was monitored by TLC, which was performed on  $2.0 \times 6.0$  cm aluminum sheets precoated with silica gel 60 (HF-254, Merck) to a thickness of 0.25 mm. The developed chromatograms were viewed under ultraviolet light (254–265 nm).

#### 4.2. General procedure for preparation of the 1,3,4-thiadiazole-2-arylhydrazone derivatives (3–15)

To a solution of 0.829 mmol of the 1,3,4-thiadiazolylhydrazone derivative (**16**) in absolute ethanol (90 mL) containing a catalytic amount of hydrochloric acid was added 0.87 mmol of corresponding aromatic aldehyde derivative. The mixture was stirred at room temperature for 30 min, when extensive precipitation was observed. The mixture was then poured into cold water, neutralized with 10% aqueous sodium bicarbonate solution. The precipitate formed was filtered out and dried, furnishing the target compounds in the yields described in Table 1.

**4.2.1. 3-Nitrobenzylidene [5-(1-methyl-5-nitro-1H-imidazol-2-yl)-1,3,4-thiadiazol-2-yl]hydrazine(3).**  $^1\text{H}$  NMR (500 MHz,  $\text{DMSO-}d_6$ )  $\delta$ : 4.37 (3H; s;  $\text{CH}_3$ ); 7.75 (1H; m; H5); 8.17 (2H; d;  $J = 8.0$  Hz; H4 and H6); 8.24 (1H; d;  $J = 2.0$  Hz; H2); 8.26 (1H; s; *H-Imidazole*); 8.51 (1H; s;  $-\text{N}=\text{CH}$ , (*E*)-diastereomer); 13.15 (1H; s; *NH*) ppm. IR ( $\text{cm}^{-1}$ ; KBr): 3135 (C–H (aromatic)); 1616 (C=NH); 1580–1472 (C=C and C=N (aromatic)); 1360–1345 (N=O).

**4.2.2. 3-Hydroxybenzylidene [5-(1-methyl-5-nitro-1H-imidazol-2-yl)-1,3,4-thiadiazol-2-yl]hydrazine(4).**  $^1\text{H}$  NMR (500 MHz,  $\text{DMSO-}d_6$ )  $\delta$ : 4.35 (3H; s;  $\text{CH}_3$ ); 6.81 (1H; dd;  $J = 8.0$  and 5.0 Hz; H4); 7.06 (1H; d;  $J = 7.6$  Hz; H6); 7.13 (1H; s; H2); 7.23 (1H; m; H5); 8.03 (1H; s;  $-\text{N}=\text{CH}$ , (*E*)-diastereomer); 8.23 (1H; s; *H-Imidazole*); 9.62 (1H; s; *NH* or *OH*); 12.81 (1H; s; *NH* or *OH*) ppm. IR ( $\text{cm}^{-1}$ ; KBr): 3530 (O–H); 1600 (N=C); 1540–1405 (C=C, C=N (aromatic)); 1360 (N=O).

**4.2.3. 2,5-Dihydroxybenzylidene [5-(1-methyl-5-nitro-1H-imidazol-2-yl)-1,3,4-thiadiazol-2-yl]hydrazine(5).**  $^1\text{H}$  NMR (500 MHz,  $\text{DMSO-}d_6$ )  $\delta$ : 4.37 (3H; s;  $\text{CH}_3$ ); 6.70–6.75 (2H; m; H3 and H4); 7.09 (1H; d;  $J = 2.8$  Hz; H6); 7.13 (1H; s; H2); 8.19 (1H; s; *H-Imidazole*); 8.40 (1H; s;  $-\text{N}=\text{CH}$ , (*E*)-diastereomer) ppm. IR ( $\text{cm}^{-1}$ ; KBr): 3530 (O–H); 1603 (N=C); 1540–1410 (C=C, C=N (aromatic)); 1363 (N=O).

**4.2.4. 2-Chlorobenzylidene [5-(1-methyl-5-nitro-1H-imidazol-2-yl)-1,3,4-thiadiazol-2-yl]hydrazine(6).**  $^1\text{H}$  NMR (500 MHz,  $\text{DMSO-}d_6$ )  $\delta$ : 4.37 (3H; s;  $\text{CH}_3$ ); 7.41–7.52

(2H; m; H3 and H6); 7.24 (1H; m; H4); 7.85 (1H; m; H5); 8.26 (1H; s; *H-Imidazole*); 8.34 and 8.50 (1H; s;  $-\text{N}=\text{CH}$ , (*Z*) and (*E*)-diastereomer, respectively); 13.10 (1H; s; *NH*) ppm. IR ( $\text{cm}^{-1}$ ; KBr): 3137–3053 (C–H (aromatic)); 1601 (C=NH); 1558–1466 (C=C and C=N (aromatic)); 1362 (N=O).

**4.2.5. 3-Chlorobenzylidene [5-(1-methyl-5-nitro-1H-imidazol-2-yl)-1,3,4-thiadiazol-2-yl]hydrazine(7).**  $^1\text{H}$  NMR (500 MHz,  $\text{DMSO-}d_6$ )  $\delta$ : 4.42 (3H; s;  $\text{CH}_3$ ); 7.47 (2H; m; H4 and H6); 7.65–7.67 (1H; m; H5); 7.73 (1H; s; H2); 8.16 (1H; s;  $-\text{N}=\text{CH}$ , (*E*)-diastereomer); 8.20 (1H; s; *H-Imidazole*); 8.27 (1H; s; *NH* or *OH*) ppm. IR ( $\text{cm}^{-1}$ ; KBr): 3135–3055 (C–H (aromatic)); 1602 (C=NH); 1557–1467 (C=C and C=N (aromatic)); 1360 (N=O).

**4.2.6. 2,3-Dihydroxybenzylidene [5-(1-methyl-5-nitro-1H-imidazol-2-yl)-1,3,4-thiadiazol-2-yl]hydrazine(8).**  $^1\text{H}$  NMR (500 MHz,  $\text{DMSO-}d_6$ )  $\delta$ : 4.36 (3H; s;  $\text{CH}_3$ ); 6.72 (1H; m; H5); 6.85 (1H; dd;  $J = 6.0$  and 1.2 Hz; H6); 7.10 (1H; dd;  $J = 6.0$  and 1.2 Hz; H4); 8.18 (1H; s; *H-Imidazole*); 8.46 (1H; s;  $-\text{N}=\text{CH}$ , (*E*)-diastereomer); 9.22 (2H; s; *NH* and *OH*) ppm. IR ( $\text{cm}^{-1}$ ; KBr): 3535 (O–H); 1610 (N=C); 1540–1410 (C=C, C=N (aromatic)); 1360 (N=O).

**4.2.7. 2,4-Dinitrobenzylidene [5-(1-methyl-5-nitro-1H-imidazol-2-yl)-1,3,4-thiadiazol-2-yl]hydrazine(9).**  $^1\text{H}$  NMR (500 MHz,  $\text{DMSO-}d_6$ )  $\delta$ : 4.37 (3H; s;  $\text{CH}_3$ ); 8.27 (1H; s; *H-Imidazole*); 8.32 (1H; d;  $J = 8.8$  Hz; H6); 8.55 (1H; dd;  $J = 8.0$  and 2.3 Hz; H5); 8.58 (1H; s;  $-\text{N}=\text{CH}$ , (*E*)-diastereomer); 8.79 (1H; d;  $J = 2.3$  Hz; H2) ppm. IR ( $\text{cm}^{-1}$ ; KBr): 3138 (C–H (aromatic)); 1610 (C=NH); 1583–1470 (C=C and C=N (aromatic)); 1360–1345 (N=O).

**4.2.8. 3-Bromobenzylidene [5-(1-methyl-5-nitro-1H-imidazol-2-yl)-1,3,4-thiadiazol-2-yl]hydrazine (10).**  $^1\text{H}$  NMR (500 MHz,  $\text{DMSO-}d_6$ )  $\delta$ : 4.37 (3H; s;  $\text{CH}_3$ ); 7.41 (1H; m; H5); 7.60 (1H; dd;  $J = 6.0$  and 2.3 Hz; H4); 7.70 (1H; d;  $J = 6.0$  Hz; H6); 7.87 (1H; s; H2); 8.15 (1H; s;  $-\text{N}=\text{CH}$ , (*E*)-diastereomer); 8.20 (1H; s; *H-Imidazole*) ppm. IR ( $\text{cm}^{-1}$ ; KBr): 3170–3055 (C–H (aromatic)); 1590–1471 (C=C and C=N (aromatic)); 1362 (N=O).

**4.2.9. 2-Nitrobenzylidene [5-(1-methyl-5-nitro-1H-imidazol-2-yl)-1,3,4-thiadiazol-2-yl]hydrazine (11).**  $^1\text{H}$  NMR (500 MHz,  $\text{DMSO-}d_6$ )  $\delta$ : 4.37 (3H; s;  $\text{CH}_3$ ); 7.66 (1H; m; H6); 7.80 (1H; m; H3); 8.05 (2H; m; H4 and H5); 8.26 (1H; s; *H-Imidazole*); 8.53 (1H; s;  $-\text{N}=\text{CH}$ , (*E*)-diastereomer); 13.20 (1H; s; *NH*) ppm. IR ( $\text{cm}^{-1}$ ; KBr): 3135 (C–H (aromatic)); 1610 (C=NH); 1580–1470 (C=C and C=N (aromatic)); 1360–1345 (N=O).

**4.2.10. 2,4-Dichlorobenzylidene [5-(1-methyl-5-nitro-1H-imidazol-2-yl)-1,3,4-thiadiazol-2-yl]hydrazine (12).**  $^1\text{H}$  NMR (500 MHz,  $\text{DMSO-}d_6$ )  $\delta$ : 4.37 (3H; s;  $\text{CH}_3$ ); 7.51 (1H; dd;  $J = 9.2$  and 2.0 Hz; H5); 7.73 (1H; d;  $J = 2.0$  Hz; H3); 7.95 (1H; d;  $J = 8.8$  Hz; H6); 8.26 (1H; s; *H-Imidazole*); 8.44 (1H; s;  $-\text{N}=\text{CH}$ , (*E*)-diastereomer) ppm. IR ( $\text{cm}^{-1}$ ; KBr): 3130–3057 (C–H (aromatic));

1600 (C=NH); 1560–1468 (C=C and C=N (aromatic)); 1360 (N=O).

**4.2.11. 2-Bromobenzylidene [5-(1-methyl-5-nitro-1H-imidazol-2-yl)-1,3,4-thiadiazol-2-yl]hydrazine (13).** <sup>1</sup>H NMR (500 MHz, DMSO-*d*<sub>6</sub>)  $\delta$ : 4.37 (3H; s; CH<sub>3</sub>); 7.40–7.51 (2H; m; H3 and H6); 7.71 (1H; m; H4); 7.94 (1H; m; H5); 8.27 (1H; s; H-Imidazole); 8.34 and 8.48 (1H; s; –N=CH, (*Z*) and (*E*)-diastereomer, respectively); 13.10 (1H; s; NH) ppm. IR (cm<sup>-1</sup>; KBr): 3170–3055 (C–H (aromatic)); 1590–1473 (C=C and C=N (aromatic)); 1360 (N=O).

**4.2.12. 2,3-Dichlorobenzylidene [5-(1-methyl-5-nitro-1H-imidazol-2-yl)-1,3,4-thiadiazol-2-yl]hydrazine (14).** <sup>1</sup>H NMR (500 MHz, DMSO-*d*<sub>6</sub>)  $\delta$ : 4.37 (3H; s; CH<sub>3</sub>); 7.46 (1H; m; H5); 7.71 (1H; dd; *J* = 6.0 and 1.2 Hz; H4); 7.93 (1H; d; *J* = 7.5 Hz; H6); 8.26 (1H; s; H-Im); 8.52 (1H; s; –N=CH, (*E*)-diastereomer); 13.20 (1H; s; NH) ppm. IR (cm<sup>-1</sup>; KBr): 3134–3052 (C–H (aromatic)); 1600 (C=NH); 1555–1470 (C=C and C=N (aromatic)); 1360 (N=O).

**4.2.13. 4-Hydroxy-3-methoxy-5-nitrobenzaldehyde [5-(1-methyl-5-nitro-1H-imidazol-2-yl)-1,3,4-thiadiazol-2-yl]hydrazine (15).** <sup>1</sup>H NMR (500 MHz, DMSO-*d*<sub>6</sub>)  $\delta$ : 3.95 (1H, s, OCH<sub>3</sub>); 4.40 (3H; s; CH<sub>3</sub>); 7.53 (1H, s, H2); 7.74 (1H, s, H6); 8.09 (1H; s; H-Imidazole); 8.23 (1H; s; –N=CH, (*E*)-diastereomer); 12.92 (1H, s, NH) ppm. IR (cm<sup>-1</sup>; KBr): 3138 (C–H (aromatic)); 1610 (C=NH); 1583–1470 (C=C and C=N (aromatic)); 1360–1345 (N=O).

## 5. Trypanocidal activity

Bloodstream trypomastigotes of the Y strain<sup>19</sup> were resuspended to a concentration of  $10 \times 10^6$  cells/mL in Dulbecco's modified Eagle's medium plus 10% fetal calf serum. This suspension (100  $\mu$ L) was added to the same volume of each compound, previously prepared at twice the desired final concentrations. Incubation was performed in 96-well microplates at 37 °C for 1 day. Untreated and megalol-treated parasites were used as controls. The final concentration of DMSO did not exceed 0.2%, which caused no damage to the parasites.<sup>17</sup> Cell counts were performed in Neubauer chamber and the activity of the compounds was expressed as IC<sub>50</sub>/1 day corresponding to the concentration that led to 50% lysis of the parasites.

## 6. Molecular modeling

Structural manipulations were performed using SYBYL 7.3 with standard Tripos force field.<sup>21</sup> Structures of the 23 megalol analogues were generated using the Build Module, available in Spartan'04, 1.0.1 version.<sup>25</sup> The imine double CH=N bond were considered as *E*-diastereomers, in agreement with X-Ray and NMR studies. The geometries of the compounds were energy optimized using MMFF and conformational analysis was performed using the same force field.<sup>26</sup> The lowest-energy

conformer of each compound was then reoptimized with the semi-empirical molecular orbital method AM1 using the MOPAC package [available in Spartan [25]].<sup>27</sup> Finally, for CoMFA studies, AM1 charges were assigned.<sup>28</sup>

## 7. CoMFA 3D-QSAR

The CoMFA method was applied to the training set for the 3D-QSAR analysis.<sup>28</sup> The steric (Lennard–Jones) and electrostatic (Coulomb) CoMFA fields were calculated at all intersections in a regularly spaced grid ranging from 1 to 2 Å within a predefined region. The steric and electrostatic interaction energies between a probe atom and the molecules were calculated using a sp<sup>3</sup> carbon as the steric probe atom and a +1.00 charge for the electrostatic probe. Cutoff values have been varied to adequately weigh steric and electrostatic contributions. The regression analysis was carried out using the full cross-validated partial least-squares<sup>28</sup> (PLS) method (leave-one-out) with CoMFA standard options for scaling of variables. To perform the PLS, column filtering value was varied from 1.0 to 6.0 kcal/mol and the number of components was varied from 1 to 6. Additional CoMFA region focusing has been applied and the weighting factor has been varied from 0.1 to 0.5, for model refinement.

Supplementary data containing the molecular structures present in the training and test set, along with other statistical details, have been provided.

## 8. Lipinski's rule of five

CLOGP, the log of the octanol/water partition coefficient, was calculated with the CLOGP software.<sup>24,29</sup>

## 9. X-ray studies

### 9.1. Crystal data

C<sub>15</sub>H<sub>12</sub>N<sub>4</sub>S, pale yellow, *M* = 280.35, *T* = 120 (2)K, monoclinic, space group P21/*c*, *a* = 13.9586 (6), *b* = 5.7280 (2), *c* = 18.1247 (7) Å,  $\beta$  = 111.198 (2)°, *V* = 1351.11 (9) Å<sup>3</sup>, *Z* = 4, *D*<sub>x</sub> = 1.378 g cm<sup>-3</sup>, monochromated Mo-K $\alpha$  radiation,  $\lambda$  = 0.71073 Å,  $\mu$  = 0.234 mm<sup>-1</sup>.

### 9.2. Data collection

The unit cell and intensity data were collected on a Bruker–Nonius diffractometer. 513515 reflections were collected, of which 3089 [*R*<sub>(int)</sub> = 0.0692] were independent reflections, with the  $2\theta$  range for data collection of 3.13–27.50°.

### 9.3. Structure solution and refinement

Structure solution and refinement were achieved using SHELX97 and SHELXL97.<sup>30</sup> Full matrix least squares on *F*<sup>2</sup> of data converged to *R*1 = 0.0833, *wR*2 = 0.1596 [*I* > 2 $\sigma$ ]. Atomic coordinates, bond lengths, angles,



and thermal parameters have been deposited at the Cambridge Crystallographic Data Center, deposition number CCDC 644660.

### Acknowledgments

This work was supported by grants from CNPq, FAPERJ, Papes/FIOCRUZ and DECIT/SCTIE/MS. The authors also thank the EPSRC X-ray Crystallographic Service, University of Southampton, England, for the data collections.

### Supplementary data

Supplementary data associated with this article can be found, in the online version, at [doi:10.1016/j.bmc.2007.09.027](https://doi.org/10.1016/j.bmc.2007.09.027).

### References and notes

1. Pink, R.; Hudson, A.; Mouries, M-A.; Bending, M. *Nat. Rev. Drug Discovery* **2005**, *4*, 727–740.
2. Croft, S.; Barrett, M. P.; Urbina, J. A. *Trends Parasitol.* **2005**, *21*, 508–512.
3. Berkelhammer, G.; Asato, G. *Science* **1968**, *162*, 1146.
4. Filardi, L. S.; Brener, Z. *Ann. Trop. Med. Parasitol.* **1982**, *76*, 293–297.
5. European Cooperation in the Field of Scientific and Technical Research, Chemotherapy of Protozoal Infections, Action B9, 2002, <http://lcost.cordis.lulsrclhome.cfm>.
6. Viodé, C.; Bettache, N.; Cenas, N.; Krauth-Siegel, R. L.; Chauviere, G.; Bakalara, N.; Perié, J. *Biochem. Pharmacol.* **1999**, *57*, 549–557.
7. Maya, J. D.; Bollo, S.; Nunez-Vergara, L. J.; Squella, J. A.; Repetto, Y.; Morello, A.; Perie, J.; Chauviere, G. *Biochem. Pharmacol.* **2003**, *65*, 999–1006.
8. Bollo, S.; Nunez-Vergara, L. J.; Bontá, M.; Chauviere, G.; Perié, J.; Squella, J. A. *J. Electroanal. Chem.* **2001**, *511*, 46–54.
9. Declerck, P. J.; De Ranter, C. J. *Biochem. Pharmacol.* **1986**, *35*, 59–61.
10. Declerck, P. J.; De Ranter, C. J. *J. Chem. Soc., Faraday Trans. 1* **1987**, *83*, 257–265.
11. Nessler, F.; Brugier, S.; Mouries, M. A.; Le Curieux, F.; Marzin, D. *Mutat. Res.* **2004**, *560*, 147–158.
12. Poli, P.; de Mello, M. A.; Buschini, A.; Mortara, R. A.; de Albuquerque, C. N.; Silva, S.; Rossi, C.; Zucchi, T. M. A. D. *Biochem. Pharmacol.* **2002**, *64*, 1617–1627.
13. Chauviere, G.; Bouteille, B.; Enanga, B.; de Albuquerque, C.; Croft, S. L.; Dumas, M.; Perié, J. *J. Med. Chem.* **2003**, *46*, 427–440.
14. Boechat, N.; Carvalho, A. S.; Fernandez-Ferreira, E.; Soares, R. O.; Souza, A. S.; Gibaldi, D.; Bozza, M.; Pinto, A. C. *Cytobios* **2001**, *105*, 83–90.
15. Carvalho, A. S.; Gibaldi, D.; Pinto, A. C.; Bozza, M.; Boechat, N. *Lett. Drug Des. Discovery* **2006**, *3*, 98–101.
16. Carvalho, A. S.; Menna-Barreto, R. F. S.; Romeiro, N. C.; deCastro, S. L.; Boechat, N. *Med. Chem.* **2007**, *3*, 460–465.
17. Carvalho, A. S.; da Silva, E. F.; Santa-Rita, R. M.; de Castro, S. L.; Fraga, C. A. M. *Bioorg. Med. Chem. Lett.* **2004**, *14*, 5967–5970.
18. Spek, A. L. *J. Appl. Cryst.* **2003**, *36*, 7–13.
19. Silva, L. H. P.; Nussenzweig, V. *Folia Clin. Biol.* **1953**, *20*, 191–208.
20. Cramer, R. D.; Patterson, D. E.; Bunce, J. *J. Am. Chem. Soc.* **1988**, *110*, 5959–5967.
21. SYBYL, Tripos Associates, 1699 South Hanley Road, Suite 303, St. Louis, Missouri 63144.
22. Böhm, M.; Stuerzebecher, J.; Klebe, G. *J. Med. Chem.* **1999**, *42*, 458–477.
23. Lipinski, C. A.; Lombardo, F.; Dominy, B. W.; Feeney, P. J. *Adv. Drug Deliv. Rev.* **1997**, *23*, 3–25.
24. Lipinski, C. A. *Drug Discov. Today: Technol.* **2004**, *1*, 337–341.
25. Spartan'04; Wavefunction, Inc. 18401 Von Karman Avenue, Suite 370. Irvine, California 92612 USA.
26. Halgren, T. A. *J. Comp. Chem.* **1996**, *17*, 490–519.
27. Dewar, M. J. S.; Zoebisch, E. G.; Healy, E. F.; Stewart, J. J. P. *J. Am. Chem. Soc.* **1985**, *107*, 3902–3909.
28. Clark, M.; Cramer, R. D., III *Quant. Struct.-Act. Relat.* **1993**, *12*, 137–145.
29. BioByte Corp. 201 W. Fourth Street, Suite #204 Claremont, CA 91711-4707; USA.
30. Sheldrick, G. M. *SHELXS97* and *SHELXL97*; University of Göttingen: Germany, 1997.